CHEMISTRY
A EUROPEAN JOURNAL

DOI: 10.1002/chem.201100577

Photoelectrochemistry of Free-Base-Porphyrin-Functionalized Zinc Oxide Nanoparticles and Their Applications in Biosensing

Wenwen Tu, Jianping Lei,* Peng Wang, and Huangxian Ju*[a]

Abstract: The photoelectrochemical properties of free-base-porphyrin-functionalized zinc oxide nanoparticles were studied. A universal photoelectrochemical biosensing platform was constructed on indium tin oxide (ITO) by using the functional nanohybrid. The nanohybrid was synthesized by means of dentate binding of ZnO nanoparticles with carboxylic groups of 4,4′,4″,4‴-(21*H*,23*H*-porphine-5,10,15,20-tetrayl)tetrakis(benzoic acid) (TCPP), and characterized with scanning electron microscopy, contact angle measurement, and spectral techniques. The nanohybrid-coated ITO electrode showed an efficient photocurrent response under irradiation at a wavelength of 360 nm, which could be greatly improved upon addition of cysteine by its oxidation at +0.3 V. The possible mechanism was that cysteine acts as a sacrificial electron donor to scavenge the photogenerated holes that locate on the excited state of TCPP, which then injects the photoexcitation electrons into the conduction band of ZnO nanoparticles, thereby transferring photoinduced electrons to the ITO electrode. Based on this enhanced photocurrent signal, a novel method for photoelectrochemical detection of cysteine was developed with a linear range of 0.6 to 157 μmol L^{-1} in physiological media. The detection limit was 0.2 μmol L^{-1} at a signal-to-noise ratio of 3. The novel strategy of cysteine analysis could provide an alternative method for monitoring biomolecules and extend the application of porphyrin-functionalized semiconductor nanoparticles.

Keywords: biosensors · nanostructures · photoelectrochemistry · porphyrinoids · zinc

Introduction

Zinc oxide (ZnO) nanoparticles have emerged as a fascinating metal oxide semiconductor nanomaterial in solar cells, due to their wide bandgap as well as excellent thermal, chemical, and structural features.[1–5] For example, direct grafting of dye onto ZnO nanorods leads to efficient electron injection from the dye after light absorption into the ZnO nanorods for additional photocurrent generation.[2] The dye-sensitized nanostructured ZnO solar cells can give a photoresponse with solar-cell efficiencies of 0.1 and 0.6% for ZnO nanorod arrays and ZnO colloid films, respectively.[3] Although the conversion efficiencies of 0.1–5.8% obtained for ZnO are much lower than that of 11% for TiO_2, ZnO has higher electronic mobility that would be favorable for electron transport and easier for fabrication on nanometer scales relative to TiO_2.[6] Therefore, it is of significant potential application in electronics, optics, and photocatalysis. In particular, these advantages of ZnO can be utilized in photoelectrochemical detection.

Photoelectrochemistry is a promising analytical technique that employs current as a detection signal with light as an excitation source.[7–10] Under illumination, semiconductor nanoparticles are first irradiated to produce holes, and the biomolecules as analyte then donate electrons to capture the holes, which leads to a relatively lower oxidation potential than direct electrochemical oxidation. This technique is sensitive due to the low background, which results from the separation of excitation source from the detection signal, and thus has been utilized for bioanalysis of proteins and small biomolecules. Some photoelectrochemical materials such as TiO_2, SnO_2, CdS, and CdSe semiconductor nanoparticles have been used for this purpose.[8–14] For instance, a photoelectrochemical immunosensor has been designed for the detection of α-Synuclein using Au-doped TiO_2 nanotube arrays.[8] A highly sensitive photoelectrochemical sensor based on a SnO_2-nanoparticle-modified indium tin oxide (ITO) electrode has been developed for the detection of adenosine triphosphate (ATP) in the extracts of cancer cells.[10] The photoelectrochemistry of CdS nanoparticles has been used for detection of tyrosinase activity.[11] Our previous work assembled an iron–porphyrin-containing sulfonic group on TiO_2 nanoparticles to develop a photoelectrochemical biosensing method for glutathione detection.[14]

Porphyrins are the mimics of many enzymes. Metalloporphyrins such as iron–porphyrin, cobalt–porphyrin, and manganese–porphyrin exhibited good electrocatalysis toward many small molecules related to life processes.[15–17] However, their photochemical and photoelectrochemical applica-

[a] W. Tu, Prof. J. Lei, P. Wang, Prof. H. Ju
MOE Key Laboratory of Analytical Chemistry for Life Science
School of Chemistry and Chemical Engineering
Nanjing University, Nanjing 210093 (P.R. China)
Fax: (+86) 25-8359-3593
E-mail: hxju@nju.edu.cn
jpl@nju.edu.cn

tions are limited due to the inhibitive transition from $3a_{2u}$ (π) to $4e_g$ (π^*) in the presence of these central metal ions.[18] In contrast, free-base porphyrin and zinc–porphyrin are good alternatives with good photochemical and photoelectrochemical properties since they have ultrafast electron injection, slow charge recombination kinetics, and high absorption coefficients.[19–22] Moreover, a porphyrin-containing carboxylic or sulfonic groups can spontaneously adsorb onto ZnO nanoparticles by bridging, ester-like, or bidentate binding.[2,14,23–25] The carboxylic-group-containing porphyrins possess a higher solar-energy conversion efficiency than sulfonic-group-containing porphyrins in dye-sensitized solar cells due to their stronger absorption coefficient.[2–5,25] Therefore, this work used carboxylic-group-containing free-base porphyrins to functionalize ZnO nanoparticles for sensitizing the photoelectrochemical efficiency of ZnO nanoparticles, which produced a universal photoelectrochemical biosensing platform.

Cysteine is an essential sulfur-containing amino acid in natural proteins.[26,27] Deficiency of cysteine leads to many diseases, such as slow growth, leucocyte loss, and liver, edema, muscle, and skin lesions.[28,29] The level of cysteine in vivo has been recognized as an important indicator for disease diagnosis.[30] Some methods have been developed for its detection, including circular dichroism spectroscopy,[30] spectrofluorimetry,[31–39] UV-visible absorption spectroscopy,[40–44] mass spectrometry,[45] and electrochemical techniques.[46–50] The main problem of the electrochemical methods is the high overpotential for oxidation of cysteine.[46,48,49] In this work, cysteine was used as an analyte model of the biosensing platform. It acted as an electron donor at relatively low potential to capture the hole of the excited 4,4′,4″,4‴-(21*H*,23*H*-porphine-5,10,15,20-tetrayl)tetrakis(-benzoic acid) (TCPP), which then injects the photoexcitation electron into the conduction band (CB) of ZnO nanoparticles to induce the electron transfer to the ITO electrode, thus leading to an enhanced photocurrent signal and a novel photoelectrochemical biosensor for cysteine (Scheme 1). This work opens up a new perspective for the photoelectrochemical application of porphyrin-functionalized semiconductor nanoparticles.

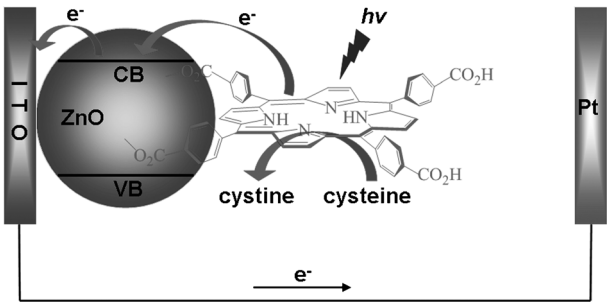

Scheme 1. Schematic illustration of the photoelectrochemical process for oxidation of cysteine at the TCPP–ZnO-modified ITO electrode (VB = valence band).

Results and Discussion

SEM images of TCPP–ZnO: SEM images of ZnO nanoparticles showed porous, microsized spherical aggregates with dense packing on the surface (Figure 1A), whereas TCPP–ZnO nanohybrids displayed a well-dispersed hexagonal starlike morphology (Figure 1B). After magnification of the SEM image (inset in Figure 1B), TCPP–ZnO nanohybrids showed an average diagonal distance of 430 nm. The decline in aggregation and the homogeneous surface structure were favorable for improving the photocurrent conversion efficiency. The hexagonal starlike structure could facilitate the accessibility of the substrate to small biomolecules, which resulted in a good photoelectrochemical response.

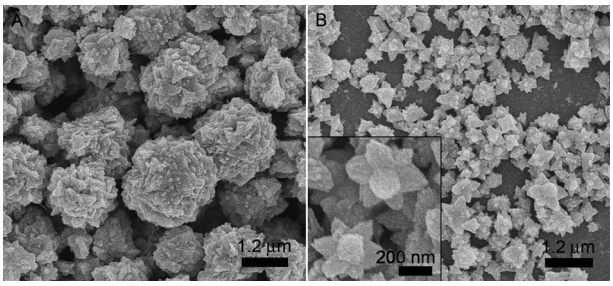

Figure 1. SEM images of A) ZnO and B) TCPP–ZnO nanohybrids on ITO surface. Inset: magnified image of TCPP–ZnO nanohybrids.

Raman spectra of TCPP–ZnO: The Raman spectrum of TCPP did not show an obvious adsorption peak in the wavenumber range of 276–640 cm^{-1} (Figure 2A, curve a). Nevertheless, four vibration peaks at 333, 384, 439, and 579 cm^{-1} could be observed in the Raman spectrum of ZnO (Figure 2A, curve b), thus indicating the presence of wurtzite structure.[51] The peaks at 384 and 579 cm^{-1} corresponded to the polar transverse A_1 and longitudinal E_1 optical phonon mode, respectively; the peak at 333 cm^{-1} was attributed to the E_2^{high}–E_2^{low} mode;[52] and the strong peak at 439 cm^{-1} could be assigned to the nonpolar optical phonon E_2 mode of the ZnO nanoparticles at high frequency, which was associated with oxygen deficiency.[53] After binding TCPP to ZnO, these characteristic bands of ZnO slightly shifted to 329, 382, 436, and 576 cm^{-1} (Figure 2A, curve c), which is indicative of its good retention of the wurtzite structure and crystal shape. Thus the functionalization of ZnO nanoparticles with TCPP did not damage the conjugation of ZnO nanoparticles.

FTIR analysis of TCPP-ZnO: The grafting method of TCPP on ZnO was evidenced by FTIR analysis (Figure 2B). The FTIR of TCPP showed a peak at 1697 cm^{-1} due to the carboxylic group of TCPP and another peak at 1388 cm^{-1} attributed to the B_{3u} vibration of porphyrin (Figure 2B, curve a).[54] The absorption bands of ZnO at 1631 and 3425 cm^{-1} (Figure 2B, curve b) could be assigned to hydroxyl groups on the surface of the ZnO.[55] By comparing the FTIR spec-

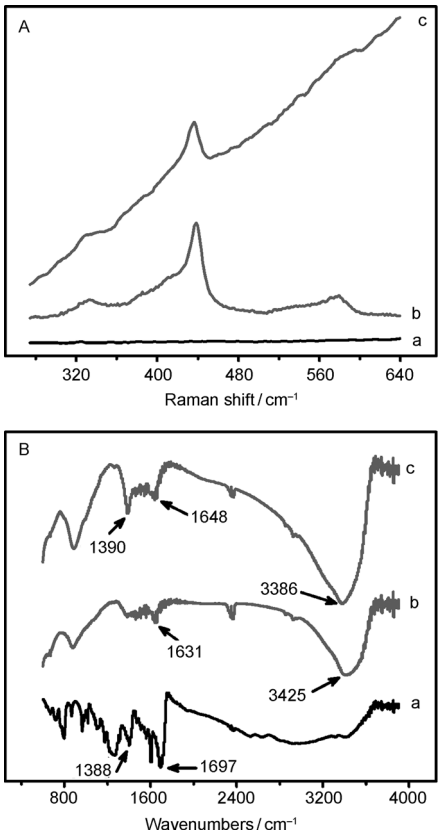

Figure 2. A) Raman and B) FTIR spectra of a) TCPP, b) ZnO, and c) TCPP–ZnO.

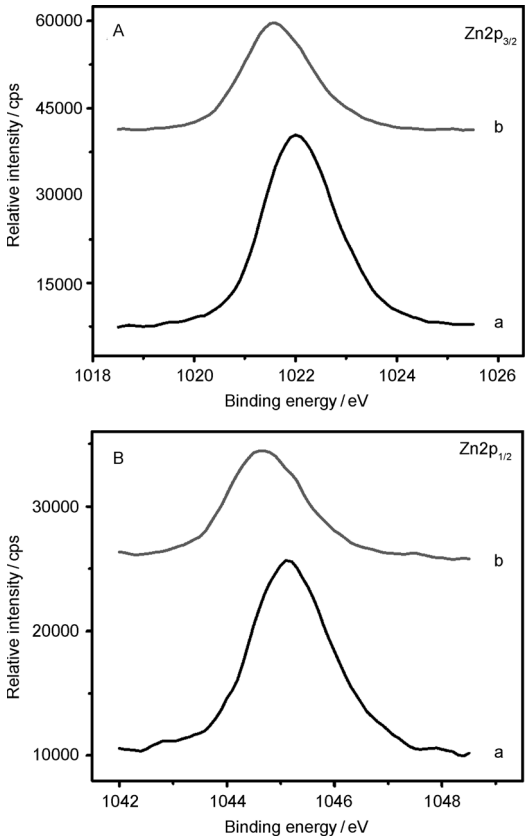

Figure 3. A) $Zn2p_{3/2}$ and B) $Zn2p_{1/2}$ XPS of a) ZnO and b) TCPP–ZnO.

tra of TCPP with TCPP–ZnO, a transformation of the carboxylic group of TCPP at 1697 cm^{-1} to typical carboxylate species with a broad band at 1648 cm^{-1} was observed (Figure 2B, curve c). Moreover, an additional peak at 1390 cm^{-1} could be observed due to the B_{3u} vibration of porphyrin on the FTIR of TCPP–ZnO. These results suggested that TCPP was successfully assembled on ZnO nanoparticles through the dentate binding of ZnO nanoparticles with the carboxylic group of TCPP.

X-ray photoelectron spectra (XPS) of TCPP–ZnO: The assembly of TCPP molecules on ZnO nanoparticles and their interaction were confirmed by XPS (Figure 3). The typical Zn2p XPS of ZnO nanoparticles showed a doublet structure due to the spin–orbit splitting, which was assigned to the $2p_{3/2}$ and $2p_{1/2}$ with a separation of binding energy 23.15 eV (Figure 3, curve a). In comparison with the Zn2p XPS of ZnO nanoparticles, the binding energy for $2p_{3/2}$ and $2p_{1/2}$ spin–orbit of the TCPP–ZnO hybrid shifted from 1021.97 and 1045.12 eV to 1021.55 and 1044.62 eV, respectively (Figure 3, curve b), thereby suggesting the existence of chemical bonds between ZnO and TCPP. The binding-energy changes were attributed to the coordination of Zn atom as an acceptor with oxygen atom as an electron donor in TCPP–ZnO.[56] These results were consistent with those from FTIR, and further confirmed that the nanohybrids of TCPP–ZnO were formed through the dentate binding between ZnO nanoparticles and TCPP.

UV/Vis absorption spectra of TCPP–ZnO: The formation of TCPP–ZnO nanohybrid was further characterized by UV spectroscopy (Figure 4). When the wavelength was above 410 nm, ZnO did not show absorption, whereas an increasing absorption occurred from 410 to 360 nm, which reached a plateau at 360 nm (Figure 4, curve a). TCPP exhibited a strong Soret absorption at 414 nm together with weak Q bands between 503 and 606 nm (Figure 4, curve b). Relative

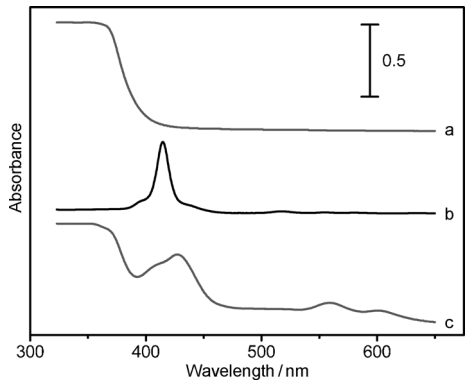

Figure 4. UV/Vis absorption spectra of a) ZnO, b) TCPP, and c) TCPP–ZnO.

to TCPP, TCPP–ZnO nanohybrid exhibited a 14 nm bathochromic shift, a broader half-bandwidth, and weaker intensity of Soret band (Figure 4, curve c). These changes were different from the absorption spectrum of *meso*-tetrakis(4-phenyl)porphyrin, which does not contain any anchoring group and did not show obvious change upon its assembly on TiO_2 nanoparticles.[25] Thus it was reasonable to conclude that TCPP–ZnO nanohybrid was formed by the interaction between the dentate binding of ZnO and carboxylic groups of TCPP rather than only physical absorption.

Time-resolved fluorescence spectra of TCPP–ZnO: The fluorescence decay curve of TCPP was fitted with single exponential decay, which showed a lifetime (τ_1) of 9.39 ns (Figure 5A). The decay curve of TCPP–ZnO showed the deviation from single-exponential decay to biexponential (Figure 5B). Two fluorescence lifetimes for grafted TCPP on ZnO and little free/physically adsorbed TCPP were obtained; they were 0.53 and 2.19 ns, respectively. The shorter lifetime was due to the binding of TCPP to ZnO. The observed decrease in lifetime could be correlated with the electron-transfer process from porphyrin molecules to ZnO nanoparticles.[25] The presence of ZnO nanoparticles would promote the interfacial photoinduced electron transfer between the excited state of TCPP and electrode surface, thereby leading to improvement of photocurrent conversion efficiency.

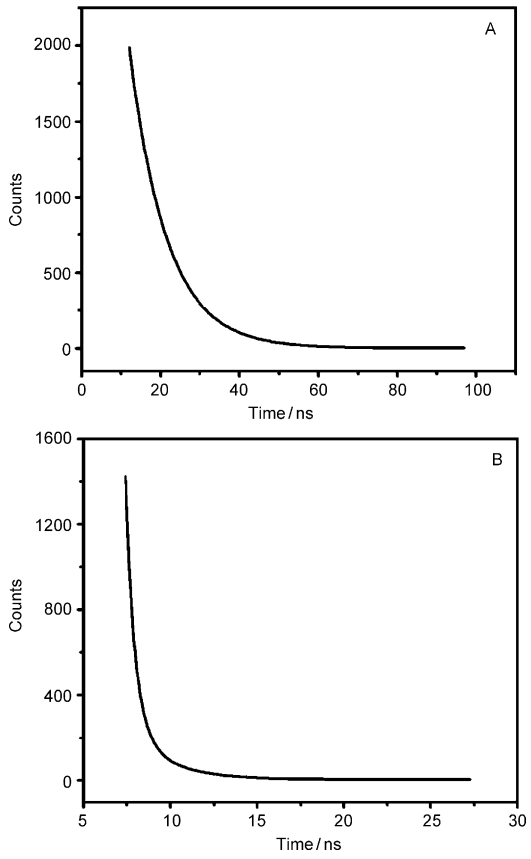

Figure 5. Time-resolved fluorescence spectra of A) TCPP and B) TCPP–ZnO suspension.

Contact-angle photographs of TCPP–ZnO: The biocompatibility of a material is positively related to its hydrophilicity, which can be characterized by the contact-angle measurement of the substrate. The bare glass slide and ZnO-nanoparticle films gave contact angles of 32.5° and 22.9°, respectively (Figure 6). The smaller contact angle of ZnO film relative to bare glass was due to some hydroxyl groups on the surface of ZnO, which was confirmed by FTIR of ZnO (Figure 2B, curve b). The TCPP–ZnO showed the minimum

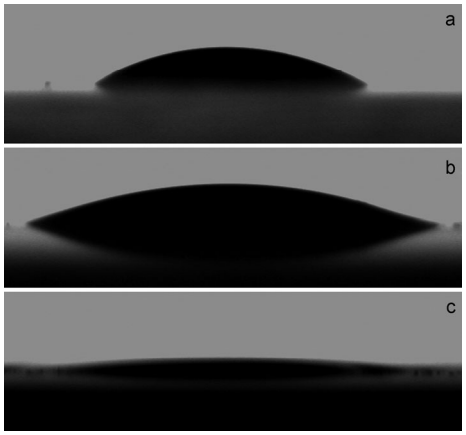

Figure 6. Contact-angle photographs of a) bare, b) ZnO, and c) TCPP–ZnO-modified substrates.

contact angle (8.4°), which was contributed to by the carboxylic acid groups introduced by water-soluble TCPP. The improved hydrophilicity and biocompatibility of the TCPP–ZnO was highly advantageous to the enhancement of the loading and reaction capacity of biomolecules and thus provided a desirable platform for photoelectrochemical biosensing and biocatalytic applications.

Photoelectrochemical response of TCPP–ZnO: The ZnO-modified ITO electrode showed a photocurrent of 4.5 nA at an applied potential of +0.3 V under illumination with light of 360 nm (Figure 7A, curve a), whereas the TCPP–ZnO-

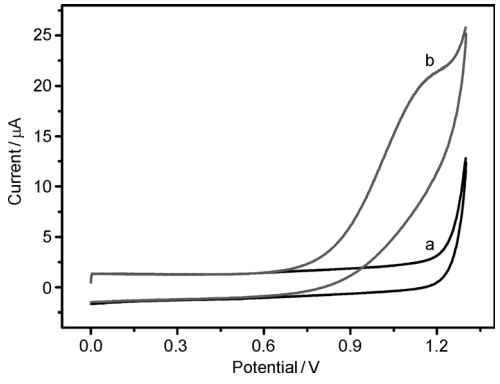

Figure 7. Photocurrent responses of A) ZnO and B) TCPP–ZnO-modified ITO electrodes in 0.1 M pH 7.0 PBS in the a) absence and b) presence of 10 mmol L^{-1} cysteine at +0.3 V to a light excitation at 360 nm.

modified ITO electrode showed a photocurrent of 7.1 nA (Figure 7B, curve a) under the same conditions. The enhanced photocurrent was due to the generated electron–hole pairs of TCPP–ZnO by excitation and their instantaneous separation from each other. The electrons could transfer from excited TCPP to the conduction band of ZnO due to the higher energy level of the excited state of TCPP than that of the conduction band of ZnO[2] (Figure 8). Finally, photoexcitation electrons transfer to the ITO electrode and generate the photocurrent.

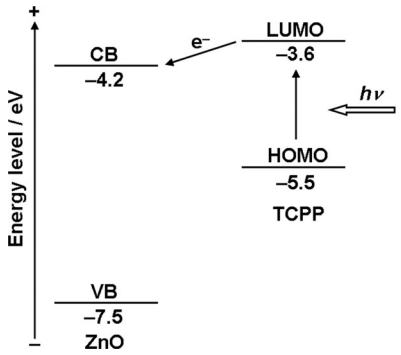

Figure 8. Schematic energy level diagram and electron-transfer path from TCPP to ZnO.

Photoelectrochemical oxidation of cysteine: When 10 μmol L^{-1} cysteine was added to the electrolyte, the photocurrent of ZnO-modified ITO electrode increased by 1.2 nA (Figure 7A, curve b), a 27% increase in photocurrent intensity. The increased photocurrent resulted from the electron injection of cysteine as an electron donor into the photogenerated holes in ZnO, in which cysteine was oxidized to form cystine.[48]

The photocurrent of TCPP–ZnO-modified ITO electrode was enhanced by 35.2 nA after the addition of 10 μmol L^{-1} cysteine (Figure 7B, curve b), which was an increase of 496% in photocurrent intensity. The much larger increase relative to that of the ZnO-modified ITO electrode was due to the different photoelectrochemical process. Here cysteine could capture the hole of the excited-state TCPP, restrain the electron–hole recombination, and inhibit the photocorrosion of TCPP.[57] The enhanced current was relatively stable over time and could be turned on and off by controlling the light. Moreover, the presence of TCPP promoted charge separation and interfacial photoinduced hole transfer. The enhanced photocurrent could be applied to the detection of cysteine, thus leading to a sensitive photoelectrochemical biosensor.

The cyclic voltammogram of TCPP–ZnO-modified ITO electrode in pH 7.0 phosphate buffered saline (PBS) did not show an observable peak in the potential range of 0 to +1.3 V (Figure 9, curve a). In the presence of cysteine, the cyclic voltammogram showed an oxidation peak of cysteine at +1.2 V with the initial potential of +0.7 V (Figure 9, curve b), thereby showing a slow electron-transfer rate. Although the oxidation peak could be used for electrochemical detection of cysteine, the much higher oxidation potential than that of photoelectrochemical oxidation limited its application.

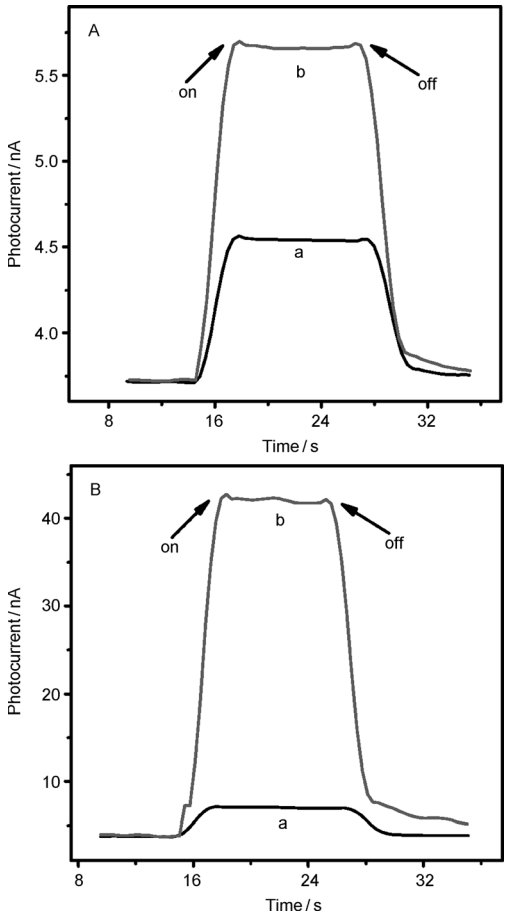

Figure 9. Cyclic voltammograms obtained at TCPP–ZnO-modified ITO electrode in 0.1 M pH 7.0 PBS in the a) absence and b) presence of 100 mmol L^{-1} cysteine at 100 mV s^{-1}.

Applied potential is an important factor relevant to the photocurrent response. As seen in Figure 10A, with an increase in potential from 0 to +0.3 V, a sharp increase of photocurrent increment was observed, which then trended a stable value. Therefore, +0.3 V was selected as the applied potential for the photoelectrochemical determination of cysteine. The potential for photoelectrochemical oxidation of cysteine at the TCPP–ZnO-modified ITO electrode was more negative than those of +0.57 V at the boron-doped diamond electrode in alkaline media,[46] +0.5 V at the β-MnO_2-nanowire-modified glassy carbon electrode (GCE) in alkaline media,[49] +0.75 V at the gallium nitride nanowire electrode,[50] and +0.35 V at the ordered mesoporous-carbon-modified glassy carbon electrode in acidic media.[48] The low applied potential was beneficial to the elimination of interference from other reductive species that coexisted in the samples.

The irradiation wavelength is another significant factor that is relevant to the photocurrent response. With an in-

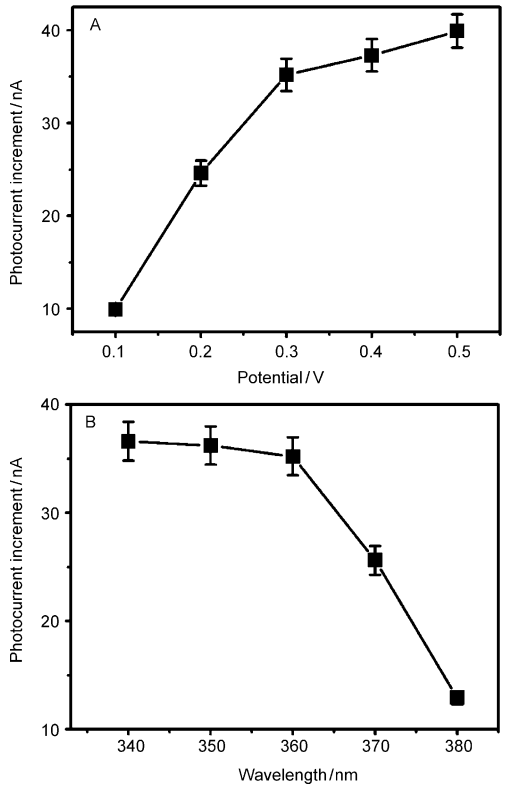

Figure 10. Effects of A) applied potential and B) excitation wavelength on the photocurrent response of TCPP–ZnO-modified ITO electrode in 0.1 M pH 7.0 PBS containing 10 mmol L^{-1} cysteine.

crease in the excitation wavelength from 340 to 360 nm at +0.3 V, the photocurrent increment leveled off and then quickly decreased from 360 to 380 nm (Figure 10B). Moreover, considering that biomolecules may suffer from irradiation with light of excessively short wavelengths, 360 nm was selected as the irradiation wavelength for the photoelectrochemical detection of cysteine.

Photoelectrochemical detection of cysteine: Figure 11 depicts the typical time-based photocurrent response of the photoelectrochemical biosensor in the presence of different concentrations of cysteine. The photocurrent intensity had a linear relationship with the concentration of the cysteine ranging from 0.6 to 157 μmol L^{-1} at +0.3 V under illumination with light of 360 nm. The linear response range of 0.6 to 157 μmol L^{-1} was wider than those of 5 to 250 μmol L^{-1} by UV absorption spectra methods,[40] 18–2500 μmol L^{-1} by electrochemical methods,[48] and 2.5 to 110 nmol L^{-1} by fluorescence spectra methods.[34] The detection limit of this method was estimated to be 0.2 μmol L^{-1} at a signal-to-noise ratio of 3. Since the normal level of cysteine in human plasma is in the range of 240–360 μmol L^{-1},[31,58,59] the present approach had enough sensitivity for the detection of cysteine in biological samples. The detection limit of 0.2 μmol L^{-1} was much lower than 39 μmol L^{-1} by fluorescence spectra methods,[38] and 0.8 μmol L^{-1} by UV absorption spectra.[44] The response could reach a steady signal

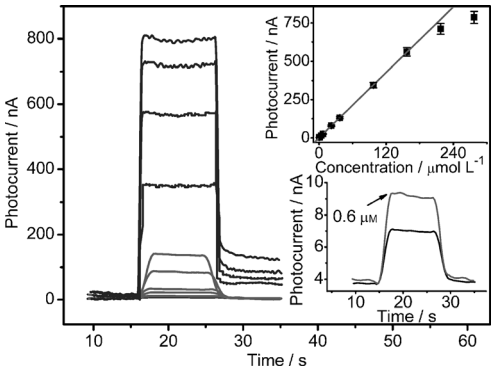

Figure 11. Photocurrent responses at TCPP–ZnO-modified ITO electrode in 0.1 M pH 7.0 PBS in the presence of 0, 0.6, 1.2, 4.2, 7.2, 22.2, 37.2, 97.2, 157, 217, and 277 mmol L^{-1} cysteine (from bottom to top) at +0.3 V to a light excitation at 360 nm. Upper inset: linear calibration curve. Lower inset: magnified response.

within only 3 s. The time for detection of cysteine was much shorter than that of 20 min for the fluorescence spectra method.[38] Therefore, the photoelectrochemical biosensor prepared with TCPP–ZnO showed a good performance for the determination of cysteine due to the effective charge separation and interfacial photoinduced hole transfer at the surface of TCPP–ZnO-modified film.

The repeatability of the photoelectrochemical biosensor was examined at the cysteine concentrations of 5 and 50 μmol L^{-1}. The relative standard deviations for four measurements were 5.6 and 5.1%, respectively, thus giving good repeatability. In addition, the slopes of the calibration plots at four freshly prepared photoelectrochemical biosensors showed the relative standard deviation of 5.3%, thereby indicating good fabrication reproducibility. After a storage time of one week in the shade at room temperature with measurements in pH 7.0 PBS every few days, no obvious decrease in the photocurrent response to cysteine was observed. After four weeks, the photocurrent response still retained 93.3% value of the initial response, thereby suggesting acceptable stability and lifetime of the immobilized TCPP–ZnO membrane.

To evaluate the selectivity of the proposed photoelectrochemical biosensing system, the effects of eight amino acids as interfering species on the photocurrent intensity of the modified electrode were examined. Proline, phenylalanine, valine, histidine, glycine, arginine, lysine, and alanine at tenfold concentration of cysteine did not affect the photoelectrochemical response of cysteine. Therefore, the as-prepared photoelectrochemical biosensor would have acceptable selectivity for monitoring of cysteine in amino acid samples.

Conclusion

A universal photoelectrochemical platform based on the nanohybrid of free-base-porphyrin-functionalized ZnO nanoparticles has been constructed on indium tin oxide for the detection of biomolecules. The TCPP–ZnO nanohybrid

is formed through the dentate binding of ZnO and carboxylic groups of TCPP rather than only physical absorption. The strong absorption coefficient of porphyrin is beneficial to improve the photocurrent conversion efficiency of metal oxide semiconductor nanoparticles. The photocurrent signal can be greatly enhanced by a sacrificial electron donor, which captures the hole of the excited-state TCPP and inhibits the photocorrosion of TCPP. The increased photocurrent leads to a photoelectrochemical biosensor for the electron donor. The proposed cysteine biosensor shows good performance such as low applied potential, rapid response, wide concentration range, low cost, and good reproducibility. The strategy provides an alternative method for monitoring biomolecules and opens up a new perspective for the photoelectrochemical application of porphyrin-functionalized semiconductor nanoparticles.

Experimental Section

Materials and reagents: 4,4′,4″,4‴-(21*H*,23*H*-porphine-5,10,15,20-tetrayl)-tetrakis(benzoic acid) (TCPP, 75%) and L-cysteine (BioUltra, $\geq$99.5%) were purchased from Sigma–Aldrich, Inc. (USA). Zinc nitrate hexahydrate ($Zn(NO_3)_2{\cdot}6H_2O$, $\geq$99%) was purchased from Xilong Chemical Co., Ltd. (China). Polyethylene glycol (formula weight 20000) was purchased from Sinopharm Chemical Reagent Co., Ltd. (China). All other chemicals were of analytical grade. Phosphate-buffered saline (PBS) (0.1 mol L^{-1}) was employed as supporting electrolyte. The pH of PBS was 7.0 unless indicated otherwise. Aqueous solutions were prepared with twice-distilled water. The photoelectrochemical system did not need deaeration.

Apparatus: SEM images were obtained using a Hitachi S-4800 SEM (Hitachi, Japan). Resonance Raman spectra were recorded using a Renishaw-inVia Raman microscope (Renishaw, United Kingdom). XPS measurements were performed using an ESCALAB 250 spectrometer (Thermo-VG Scientific, USA) with ultra-high vacuum generators. Ultraviolet-visible absorption spectra were recorded using a UV-3600 spectrometer (Shimdzu, Japan). Fourier-transform infrared spectra (FTIR) were obtained using a Nicolet iS10 instrument (Nicolet, USA). The static water contact angles were measured using a contact-angle meter (Rame-Hart-100, USA) with droplets of deionized water at 25°C. Fluorescence lifetimes were recorded at room temperature using an FLS920 fluorescence spectrometer (Edinburgh Instruments Ltd., United Kingdom). Photoelectrochemical measurements were performed using a home-built photoelectrochemical system. A 500 W Xe lamp equipped with a monochromator was used as irradiation source. Photocurrent was measured using a CHI 660D electrochemical workstation (CH Instruments Inc., USA). All experiments were carried out at room temperature using a conventional three-electrode system with a modified indium tin oxide (ITO) electrode as working, a platinum wire as auxiliary, and a saturated calomel electrode as reference electrodes.

Preparation of TCPP–ZnO and the modified ITO electrodes: $Zn(NO_3)_2{\cdot}6H_2O$ (100 mg) and polyethylene glycol (200 mg) were dissolved in twice-distilled water (30 mL). KOH (16 mL, 11 mg mL^{-1}) aqueous solution was then dropped into the solution with sonication for 2 h at 50°C. The obtained suspension was aged for 20 min at the same temperature. After the suspension was centrifuged at 8000 rpm, washed with twice-distilled water 5 times and dried, ZnO nanoparticles were obtained.

ZnO nanoparticles (10 mg) and water (5 mL) were successively added to TCPP solution (1 mL, 5 mmol L^{-1}, pH 8.0). The resulting suspension was ultrasonically dispersed for 1.5 h, and then centrifuged at 8000 rpm for 20 min to remove free TCPP. After thrice washing with water, the sediment was dried at 70°C to obtain the TCPP–ZnO nanohybrid, which was then ultrasonically dispersed in water to obtain a TCPP–ZnO suspension (2 mg mL^{-1}).

An ITO electrode was cleaned with NaOH (1 mol L^{-1}) and H_2O_2 (30%), then washed with acetone and water, and dried at room temperature. The TCPP–ZnO suspension (10 μL, 2 mg mL^{-1}) was coated onto the ITO electrode and dried in the shade at room temperature to obtain a TCPP–ZnO-modified ITO electrode. The ZnO-modified ITO electrode was prepared similarly.

Acknowledgements

This work was financially supported by the Important National S&T Specific Project (2009ZX10004-313), the National Basic Research Program of China (2010CB732400), the National Natural Science Foundation of China (20821063, 20875044, 21075060), and the Science Foundation of Jiangsu (BK2008014, BK2010302).

[1] J. F. Gnichwitz, R. Marczak, F. Werner, N. Lang, N. Jux, D. M. Guldi, W. Peukert, A. Hirsch, *J. Am. Chem. Soc.* **2010**, *132*, 17910.
[2] A. J. Said, G. Poize, C. Martini, D. Ferry, W. Marine, S. Giorgio, F. Fages, J. Hocq, J. Bouclé, J. Nelson, J. R. Durrant, J. Ackermann, *J. Phys. Chem. C* **2010**, *114*, 11273.
[3] E. Galoppini, J. Rochford, H. H. Chen, G. Saraf, Y. C. Lu, A. Hagfeldt, G. Boschloo, *J. Phys. Chem. B* **2006**, *110*, 16159.
[4] A. S. Huss, A. Bierbaum, R. Chitta, D. J. Ceckanowicz, K. R. Mann, W. L. Gladfelter, D. A. Blank, *J. Am. Chem. Soc.* **2010**, *132*, 13963.
[5] R. A. Jensen, H. V. Ryswyk, C. X. She, J. M. Szarko, L. X. Chen, J. T. Hupp, *Langmuir* **2010**, *26*, 1401.
[6] Q. F. Zhang, C. S. Dandeneau, X. Y. Zhou, G. Z. Cao, *Adv. Mater.* **2009**, *21*, 4087.
[7] N. Haddour, J. Chauvin, C. Gondran, S. Cosnier, *J. Am. Chem. Soc.* **2006**, *128*, 9693.
[8] Y. R. An, L. L. Tang, X. L. Jiang, H. Chen, M. C. Yang, L. T. Jin, S. P. Zhang, C. G. Wang, W. Zhang, *Chem. Eur. J.* **2010**, *16*, 14439.
[9] C. F. Ding, H. Li, X. L. Li, S. S. Zhang, *Chem. Commun.* **2010**, *46*, 7990.
[10] X. R. Zhang, Y. Q. Zhao, S. G. Li, S. S. Zhang, *Chem. Commun.* **2010**, *46*, 9173.
[11] H. B. Yildiz, R. Freeman, R. Gill, I. Willner, *Anal. Chem.* **2008**, *80*, 2811.
[12] Q. Kang, L. X. Yang, Y. F. Chen, S. L. Luo, L. F. Wen, Q. Y. Cai, S. Z. Yao, *Anal. Chem.* **2010**, *82*, 9749.
[13] E. Golub, G. Pelossof, R. Freeman, H. Zhang, I. Willner, *Anal. Chem.* **2009**, *81*, 9291.
[14] W. W. Tu, Y. T. Dong, J. P. Lei, H. X. Ju, *Anal. Chem.* **2010**, *82*, 8711.
[15] W. W. Tu, J. P. Lei, G. Q. Jian, Z. Hu, H. X. Ju, *Chem. Eur. J.* **2010**, *16*, 4120.
[16] W. W. Tu, J. P. Lei, S. Y. Zhang, H. X. Ju, *Chem. Eur. J.* **2010**, *16*, 10771.
[17] J. P. Collman, R. Boultaov, C. J. Sunderland, I. M. Shiryaeva, K. E. Berg, *J. Am. Chem. Soc.* **2002**, *124*, 10670.
[18] G. J. Kavarnos, N. J. Turro, *Chem. Rev.* **1986**, *86*, 401.
[19] V. Sgobba, D. M. Guldi, *Chem. Soc. Rev.* **2009**, *38*, 165.
[20] D. Baskaran, J. W. Mays, X. P. Zhang, M. S. Bratcher, *J. Am. Chem. Soc.* **2005**, *127*, 6916.
[21] D. M. Guldi, G. M. A. Rahman, F. Zerbetto, M. Prato, *Acc. Chem. Res.* **2005**, *38*, 871.
[22] C. Y. Lee, J. K. Jang, C. H. Kim, J. Jung, B. K. Park, J. Park, W. Choi, Y. K. Han, T. Joo, J. T. Park, *Chem. Eur. J.* **2010**, *16*, 5586.
[23] J. Rochford, D. Chu, A. Hagfeldt, E. Galoppini, *J. Am. Chem. Soc.* **2007**, *129*, 4655.
[24] J. Rochford, E. Galoppini, *Langmuir* **2008**, *24*, 5366.
[25] A. Kathiravan, P. S. Kumar, R. Renganathan, S. Anandan, *Colloids Surf. A* **2009**, *333*, 175.
[26] W. Dröge, V. Hack, R. Breitkreutz, E. Holm, G. Shubinski, E. Schmid, D. Galter, *Biofactors* **1998**, *8*, 97.

[27] L. P. Osman, S. C. Mitchell, R. H. Waring, *Sulfur Rep.* **1997**, *20*, 155.
[28] S. Shahrokhian, *Anal. Chem.* **2001**, *73*, 5972.
[29] V. Gazit, R. Ben-Abraham, R. Coleman, A. Weizman, Y. Katz, *Amino Acids* **2004**, *26*, 163.
[30] J. Nan, X. P. Yan, *Chem. Eur. J.* **2010**, *16*, 423.
[31] H. Y. Shiu, H. C. Chong, Y. C. Leung, M. K. Wong, C. M. Che, *Chem. Eur. J.* **2010**, *16*, 3308.
[32] C. Zhao, K. G. Qu, Y. J. Song, C. Xu, J. S. Ren, X. G. Qu, *Chem. Eur. J.* **2010**, *16*, 8147.
[33] M. Zhang, M. X. Yu, F. Y. Li, M. W. Zhu, M. Y. Li, Y. H. Gao, L. Li, Z. Q. Liu, J. P. Zhang, D. Q. Zhang, T. Yi, C. H. Huang, *J. Am. Chem. Soc.* **2007**, *129*, 10322.
[34] F. Pu, Z. Z. Huang, J. S. Ren, X. G. Qu, *Anal. Chem.* **2010**, *82*, 8211.
[35] K. S. Lee, T. K. Kim, J. H. Lee, H. J. Kim, J. I. Hong, *Chem. Commun.* **2008**, 6173.
[36] H. L. Li, J. L. Fan, J. Y. Wang, M. Z. Tian, J. J. Du, S. G. Sun, P. P. Sun, X. J. Peng, *Chem. Commun.* **2009**, 5904.
[37] Y. B. Ruan, A. F. Li, J. S. Zhao, J. S. Shen, Y. B. Jiang, *Chem. Commun.* **2010**, *46*, 4938.
[38] S. Lim, J. O. Escobedo, M. Lowry, X. Y. Xu, R. Strongin, *Chem. Commun.* **2010**, *46*, 5707.
[39] Y. K. Yang, S. Shim, J. Tae, *Chem. Commun.* **2010**, *46*, 7766.
[40] N. Shao, J. Y. Jin, S. M. Cheung, R. H. Yang, W. H. Chan, T. Mo, *Angew. Chem.* **2006**, *118*, 5066; *Angew. Chem. Int. Ed.* **2006**, *45*, 4944.
[41] P. K. Sudeep, S. T. S. Joseph, K. G. Thomas, *J. Am. Chem. Soc.* **2005**, *127*, 6516.
[42] T. Li, L. L. Shi, E. K. Wang, S. J. Dong, *Chem. Eur. J.* **2009**, *15*, 3347.
[43] X. H. Zhou, D. M. Kong, H. X. Shen, *Anal. Chem.* **2010**, *82*, 789.
[44] C. Lu, Y. B. Zu, *Chem. Commun.* **2007**, 3871.
[45] N. Burford, M. D. Eelman, D. E. Mahony, M. Morash, *Chem. Commun.* **2003**, 146.
[46] N. Spătaru, B. V. Sarada, E. Popa, D. A. Tryk, A. Fujishima, *Anal. Chem.* **2001**, *73*, 514.
[47] J. M. Zen, A. S. Kumar, J. C. Chen, *Anal. Chem.* **2001**, *73*, 1169.
[48] M. Zhou, J. Ding, L. P. Guo, Q. K. Shang, *Anal. Chem.* **2007**, *79*, 5328.
[49] Y. H. Bai, J. J. Xu, H. Y. Chen, *Biosens. Bioelectron.* **2009**, *24*, 2985.
[50] Y. T. Lai, A. Ganguly, L. C. Chen, K. H. Chen, *Biosens. Bioelectron.* **2010**, *26*, 1688.
[51] Z. H. Dai, K. Liu, Y. W. Tang, X. D. Yang, J. C. Bao, J. Shen, *J. Mater. Chem.* **2008**, *18*, 1919.
[52] R. Cuscó, E. Alarcón-Lladó, J. Ibáñez, L. Artús, J. Jiménez, B. G. Wang, M. J. Callahan, *Phys. Rev. B* **2007**, *75*, 165202.
[53] P. Jiang, J. J. Zhou, H. F. Fang, C. Y. Wang, Z. L. Wang, S. S. Xie, *Adv. Funct. Mater.* **2007**, *17*, 1303.
[54] X. X. Zhang, Y. X. Zhang, J. Z. Jiang, *Spectrochim. Acta A Mol. Biomol. Spectrosc.* **2005**, *61*, 2576.
[55] R. Wahab, S. G. Ansari, Y. S. Kim, H. K. Seo, H. S. Shin, *Appl. Surf. Sci.* **2007**, *253*, 7622.
[56] D. Li, W. J. Dong, S. M. Sun, Z. Shi, S. H. Feng, *J. Phys. Chem. C* **2008**, *112*, 14878.
[57] G. L. Wang, P. P. Yu, J. J. Xu, H. Y. Chen, *J. Phys. Chem. C* **2009**, *113*, 11142.
[58] S. Seshadri, A. Beiser, J. Selhub, P. F. Jacques, I. H. Rosenberg, R. B. D'Agostino, P. W. F. Wilson, P. A. Wolf, *N. Engl. J. Med.* **2002**, *346*, 476.
[59] H. Refsum, P. M. Ueland, O. Nygard, S. E. Vollset, *Annu. Rev. Med.* **1998**, *49*, 31.

Received: February 21, 2011
Published online: June 15, 2011

